Development of an Aerodynamic Model for a Ciclocopter

Diogo José Maurício
diogo.mauricio@tecnico.ulisboa.pt

Instituto Superior Técnico, Universidade de Lisboa, Portugal

April 2019

Abstract

In the last few years the interest for "drones" (unmanned aerial vehicles) have increased in several sectors. In the military sector, in video surveillance, in meteorology, entertainment, among others, the need to conduct a vehicle optimization was essential. The main goal of this thesis is to study the general behavior of a cyclocopter (a kind of drone whose blades/wings rotate parallel to the axis of rotation), mainly to understand the way to develop propulsion and propulsive force in this type of equipment. The fundamental structural aspects in order to build a cyclocopter among the aerodynamic aspects that govern their behavior will be introduce. The numerical models that can be applied to this type of aircraft will be explained as well as the advantages and disadvantages, and possible simplifications. By using these numerical models it will be explored the way that a cyclocopter behave (produced forces) when some of the characteristics like the angle of attack, the rotor diameter and the rotation speed are varied.

Keywords: Cyclocopter, Rotor, Unsteady Aerodynamics, Single Streamtube, Double-Multiple Streamtube

1. Introduction

In recent years the interest in unmanned aerial vehicles or, more commonly known as "drones" has increased in the most diversified sectors. Its applicability can be found in the military, security / security, meteorology, transportation, entertainment and others sectors.

The "drones", when compared to "conventional" aircraft, are, with some exceptions of smaller dimensions. They therefore have the advantage of having low operating costs (low power consumption and little or no maintenance), easy to use, and do not require, at least for now, costly licenses or "licenses" to operate them. The variety of drones is also extensive. One can find fixed and movable wing drones (flapping or rotating), but in this document will be study only movable wing drones. Its field of applicability is not yet closed, as this type of equipment can be further improved.

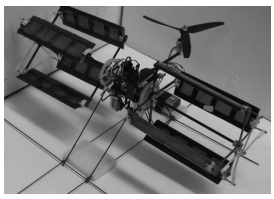

(a) Cyclorotor.

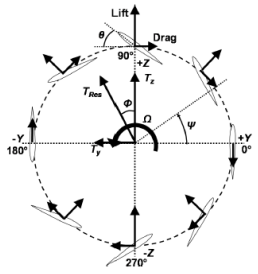

(b) Angles and vectorial forces in a cyclorotor

Figure 1: Example of a cyclorotor (a) and a scheme of vectorial forces in a cyclorotor (b) [1].

2. The cyclocopter

2.1. GeneralConcepts

A cyclorotor (also known as a cyclocopter) is a rotating wing system where the wings, or blades, rotate parallel to the axis of rotation Fig.1.

The angle of attack of each blade varies cyclically according to the mechanism mounted on the axis of rotation, such that the blades experience positive and negative angles of attack in the upper and lower positions, respectively, of each cycle. The resistance and lift forces produced along the cycle by each blade can be decomposed into a perpendicular component and a tangential to the wing profile.

2.2. Cyclocopter Blades

To study the blades deformations on the cyclorotor, these can modeled it as non-linear beams, Euler-Bernoulli isotropic, under radial bending deformations (w), tangential bending (v) and elastic torsion (ϕ). The coordinate system of the blade is shown in Fig. 2.

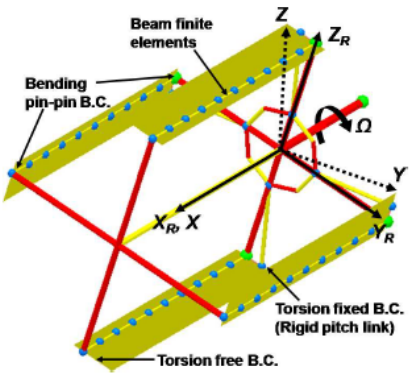

Figure 2: Coordinate system.[1].

2.3. Mechanism of Variation of Angle of Attack

For this type of cyclorotor concept to be feasible as a flying vehicle, it is important to design a mechanism of variation of the angles of attack as light and simple as possible. It is advisable that the connection between the axis of rotation and the mechanism is direct so that the only waste of power comes from the friction between the movements of the components [1].

The mechanism consists basically of two bearings in which the smallest one is inserted inside the larger bearing, as shown in Fig. 3 . These bearings are installed so that there is a spacing between them that allows a displacement, L_2, between their axes. (Fig. 4)

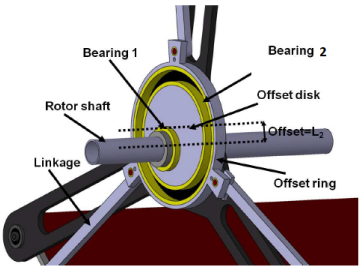

Figure 3: Mechanism's bearings and linkages [2].

Kinematics of the Blade Pitch Mechanism

The geometric angle of attack θ can be defined as the following sinusoidal function which includes the azimuth angle Ψ and the angle of eccentricity ϕ [3]:

$$\theta = -\theta_{max} sin(\Psi - \phi) \tag{1}$$

The effective angle of attack can be obtained by subtracting the induced angle of attack, α_{dw}, at the angle of geometric attack:

$$\alpha = \theta - \alpha_{dw} = sin(\Omega t - \phi) - \alpha_{dw} \tag{2}$$

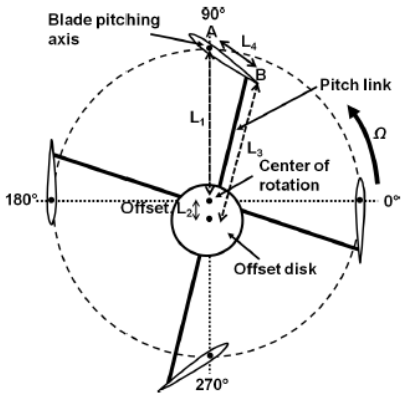

Figure 4: Operating diagram of the control mechanism with L2 Offset [2].

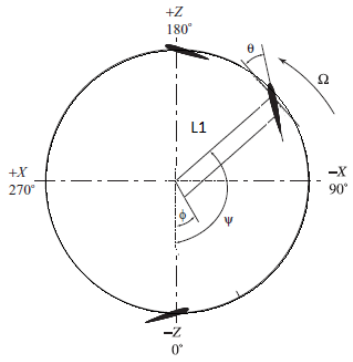

Figure 5: Coordinate System [3].

First and second derivate of the angular velocity and acceleration, respectively:

$$\dot{\theta} = -\theta_{max}\Omega cos(\Omega t - \phi) \tag{3}$$

$$\ddot{\theta} = \theta_{max}\Omega^2 sen(\Omega t - \phi) \tag{4}$$

The blade angle variation mechanism does not produce an exact sinusoid at the pitch angle. This difference affects velocity and angular acceleration which, in turn, will affect the lift's non-circulatory components. This makes it necessary to accurately calculate the kinematic equations of the pitch angle mechanism to obtain good accuracy results. To model the bar angle mechanism of the bars, which is composed of four bars, one can use the 4-bar mechanism described in [4] whose example is shown in Fig. 6.

This demonstrative example (Fig. 6 is a generic four-bar mechanism whose bars can be transposed for the case under study. Bar 4 represents the blade, bar 2 represents the previously spoken L_2 where the offset is performed Fig. 4. The bar 1 the L_1 and finally the bar 3 the L_3.

Substituting each link for a vector, we can write the

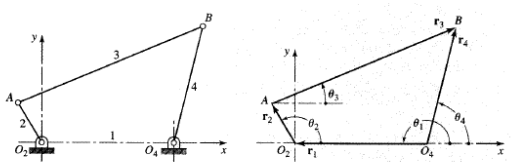

Figure 6: Four-bar mechanism [4].

following equation:

$$\vec{r}_1 + \vec{r}_2 + \vec{r}_3 - \vec{r}_4 = 0 \tag{5}$$

If one replace each vector by a complex number:

$$r_1 e^{j\theta_1} + r_2 e^{j\theta_2} + r_3 e^{j\theta_3} + r_4 e^{j\theta_4} = 0 \tag{6}$$

Since link 1 is a fixed bar, the first-order derivative of the equation 6 is:

$$jr_2\dot{\theta_2}e^{j\theta_2} + jr_3\dot{\theta_3}e^{j\theta_3} + jr_4\dot{\theta_4}e^{j\theta_4} = 0 \tag{7}$$

Developing the equation 7, detaching the real part from the imaginary and attributing $\dot{\theta_2} = \omega_2$, $\dot{\theta_3} = \omega_3$ e $\dot{\theta_4} = \omega_4$ it can be obtained, among others, the angular velocity of the link 4, corresponding to the blade:

$$\omega_4 = \frac{r_2\omega_2 sen(\theta_3 - \theta_4)}{r_4 sen(\theta_4 - \theta_3)} \tag{8}$$

Assuming that the rotor is not accelerating ($\alpha_2 = 0$), the angular acceleration is given by:

$$\alpha_4 = \frac{r_3\omega_3^2 + r_2\omega_2^2 cos(\theta_2 - \theta_3) + r_4\omega_4 cos(\theta_4 - \theta_3)}{r_4 sen(\theta_3 - \theta_4)} \tag{9}$$

all angles, speeds and accelerations are defined as positive counterclockwise.

3. Unsteady Aerodynamics

3.1. Indicial Response: Wagner Problem

The lift coefficient circulatory part, C_l^c, in response to an arbitrary variation of the angle of attack can be written as a relation to Wagner's function as [4]:

$$C_l^c(t) = 2\phi_w(\alpha(0)\phi(s) + \int_0^s \frac{d\alpha(s-\sigma)}{dt}\phi(s-\sigma)d\sigma = 2\pi\alpha_e(t) \tag{10}$$

where α_e represents the effective angle of attack and contains implicitly all the lift's effect over time (t) from wake information.

Although Wagner's function is known accurately, its analytical form does not contain an easy resolution. It is therefore common to replace it with an exponential function or algebraic approximation. One of the approximations of Wagner's function is written as an exponential function of two terms and four coefficients:

$$\phi_w(s) = 1.0 - A_1 e^{0.0455s} - A_2^{-0.3s} \Leftrightarrow \phi_w(s) = 1.0 - 0.165e^{0.0455s} - 0.335e^{-0.3s} \tag{11}$$

An alternative algebraic approach to Wagner's function is written as:

$$\phi_w(s) = \frac{s+2}{s+4} \tag{12}$$

.

3.2. Indicial Response Method

If the indicial aerodynamic response can be determined, then these solutions form a powerful mean to find the air velocity forces and moments in time domain as a result of arbitrary variations in the angle of attack and / or the velocity of the flow. The variation of the lift coefficient, $C_l(s)$, over time can be presented as a function of the angle of attack, $\alpha(s)$, in terms of Duhamel's integral as [4]:

$$C_l(s) = C_{l_\alpha}\left[\alpha(s_0)\phi_w(s) + \int_{s_0}^s \frac{d\alpha}{ds}(\sigma)\phi(s-\sigma)d\sigma\right] = C_{l\alpha}\alpha_e(s) \tag{13}$$

where $\phi_w(s)$ is the indicial response to a unitary step $C_{l\alpha}$ and is the lift curve slope, for incompressible flow. When calculating the integral, the term α_{es} can be considered as an effective angle of attack in which it's contained all its history. The equation 13 is usually solved numerically to discretized time values.

The indicial response function is also not always known analytically, as with the functions of Wagner and Krussner, and therefore a large set of numerical operations will have to be performed. Fortunately, there are alternative approaches to the problem [7].

3.3. Recursive Solution for Duhmel Integral

If an indicial exponential growth function is assumed, such that [4]:

$$\phi_w(s) = 1 - A_1 e^{-b_1 s} - A_2 e^{-b_2 s} \tag{14}$$

then Duhamel's integral of the equation (13) can be written as:

$$\alpha_e(s) = \alpha(s) - X(s) - Y(s) \tag{15}$$

where X e Y are:

$$X(s) = A_1 \int_{s_0}^s \frac{d\alpha}{ds}(\sigma)e^{-b_1(s-\sigma)}d\sigma \tag{16}$$

$$Y(s) = A_2 \int_{s_0}^s \frac{d\alpha}{ds}(\sigma)e^{-b_2(s-\sigma)}d\sigma \tag{17}$$

Assuming a sample with temporal steps, Δs and $s_0 = 0$, and expanding the integral into two parts it can be obtained:

$$X(s)e^{-b_1\Delta s} + A_1 \int_s^{s+\Delta s} \frac{d\alpha}{ds}(\sigma)e^{-b_1(s+\Delta s-\sigma)}d\sigma = X(s)e^{-b_1\Delta s} + I \tag{18}$$

Note that this new value,, $X(s + \Delta s)$, is a single-step recursive formula, related to the previous value, $X(s)$, and the new increment, I, new period resulting. Considering the term I:

$$I = A_1 e^{-b_1(s+\Delta s)} \int_s^{s+\Delta s} \frac{d\alpha}{ds}(\sigma)e^{b_1\sigma}d\sigma \\ A_1 e^{-b_1(s+\Delta s)} \int_s^{s+\Delta s} \frac{d\alpha}{ds}(\sigma)f(\sigma)d\sigma \tag{19}$$

with $f(\sigma) = e^{b_1\sigma}$. Introducing finite difference approximation for $d\alpha/ds$ time related $s + \Delta s$ it can be obtained:

$$\frac{d\alpha}{ds}\Big|_{s+\Delta s} = \frac{3\alpha(s+\Delta s) - 4\alpha(s) + \alpha(s+\Delta s)}{2\Delta s} \tag{20}$$

The remaining part of the integral involving $f(\sigma)$ can be written exactly and I it is shown as:

$$I = A_1 \left(\frac{\Delta\alpha_{s+\Delta s}}{\Delta s}\right)\left(\frac{1 - e^{-b_1\Delta s}}{b_1}\right) \tag{21}$$

If $b_1\Delta s$ take small values such that $b_1^2(\Delta s)^2$ and the higher powers can be neglected, then:

$$I = A_1 \left(\frac{\Delta\alpha_{s+\Delta s}}{\Delta s}\right)\Delta s = A_1\Delta\alpha_{s+\Delta s} \tag{22}$$

When the equation 22 is introduced in equation 18 it can be obtained the recursive form:

$$X(s) = X(s - \Delta s)e^{-b_1\Delta s} + A_1\Delta\alpha_s \tag{23}$$

Proceding in a similar way to the term Y in equation 17 and using the equation 15 it can be obtained:

$$\alpha_e(s) = \alpha(0) + \int_0^s d\alpha(s) - X(s) - Y(s) \\ = \alpha(s) - X(s) - Y(s) \tag{24}$$

where $X(s)$ e $Y(s)$ are given by the recursive form in which they are a constituent part of the calculation algorithm:

$$X(s) = X(s - \Delta s)e^{-b_1\Delta s} + A_1\Delta\alpha_s \tag{25}$$

$$Y(s) = Y(s - \Delta s)e^{-b_2\Delta s} + A_2\Delta\alpha_s \tag{26}$$

It should be noted that the recursive functions $X_{(s)}$ and $Y_{(s)}$ contain all historical information of non-stationary aerodynamics and are updated to each unit step by providing efficient numerical solutions for the lift at each arbitrary variation of the attack α.

4. Rotor Flow Models

Two different models based on internal flow and on the momentum theory are analized in this document: (i) Single streamtube model, where the entire rotor is immersed in a single flow tube as shown in 7(a) and (ii) Double-multiple streamtube model where the rotor is divided into a number of independent tubes whose upper and lower parts of each tube are studied separately. Fig.7 (b).

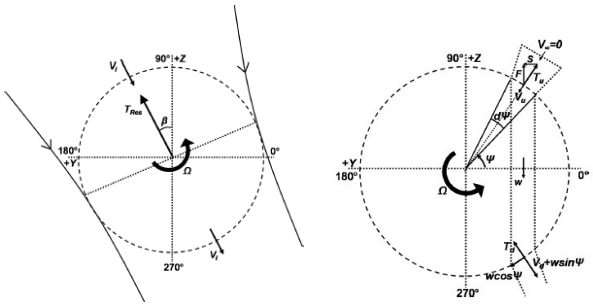

(a) Single streamtube (b) Double multipole

Figure 7: schematic flow models. [?]

4.1. Single Streamtube Model

In order to obtain a flow model it will be useful, as a starting point, the quantity of motion theorem described in [5] and shown in the equation 27.

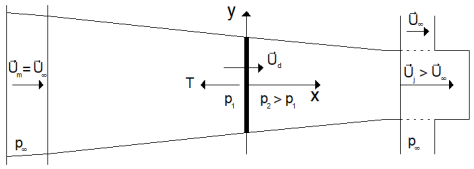

Figure 8: Streamtube on an actuator disk.

$$\oint_{SC} \rho U_i U_j n_j dS = \int_{VC} -\frac{\partial p}{\partial x_i}dV + \int_{VC} \frac{\partial \tau_{ij}}{\partial x_j}dV \\ = \oint_{SC} -pn_i dS + \oint_{SC} \tau_{ij}n_j dS \tag{27}$$

Modeling the wake's ciclocopter (Fig.9) as a single streamtube (Fig.8 [2]), and assuming: (i) a perfectly axi-symmetric simplified model; (ii) the rotor modeled as a disk with an infinite number of blades; (iii) each producing an elementary contribution to the driving force; it comes to a model called actuator disk, in which the flow results in quasi-one-dimensional [5].

Through the disk, the velocity evolution u_d is continuous, by mass conservation. The static pressure, however, accuses a discontinuity of p_1 to $p_2 > p_1$, corresponding to the energy that the fluid locally impart.

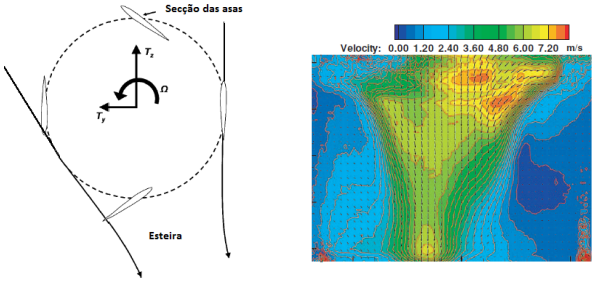

(a) Example of a wake scheme produced by the rotor.

(b) Wake's Average velocity measurements of produced by the cyclocoptero.

Figure 9: Cyclocopter's wake schematic and real models [2].

Defining the propulsive force T, both in terms of the amount of movement variation in the current tube shown in Fig. 8 and of the pressure jump through the actuator disk, always admitting a perfect fluid model and assuming the sections upstream and downstream of the streamtube sufficiently far from the actuator disk, it has: (i) null resultant force on the lateral segments of the current surface in infinite medium; (ii) $U_m = U_\infty$ and $p_m = p_\infty$, in the upstream section; (iii) in the inner downstream section of the tube (iv) $U = U_\infty$ outside the tube, (v) $p_j = p_\infty$; the equation 27 it is obtained as [5]:

$$-\rho U_\infty^2 A_i + \rho U_f^2 A_f = -T \tag{28}$$

where S_m e S_j are, respectively, the straight sections areas of the streamtube upstream and downstream of the actuator disk.

Per continuity:

$$U_\infty A_i = U_f A_f = v_i A \tag{29}$$

so that the relation for the T can be rewritten as:

$$T = \rho v_i A(U_f - U_\infty) \tag{30}$$

Resorting to algebraic manipulations in equation 30 it can be obtained:

$$T = \rho v_i A(U_f - U_\infty) = \frac{1}{2}\rho(U_f + U_\infty)(U_f - U_\infty)A \tag{31}$$

in which results:

$$v_i = \frac{U_\infty + U_f}{2} \tag{32}$$

denoting that the velocity across the disk is the velocities arithmetic mean, at infinity, upstream and downstream.

The propulsive power or useful power of the propeller is expressed as the work of the propelling force per unit of time, meaning:

$$P_{util} = TU_\infty = \rho v_i A(U_f - U_\infty)U_\infty \tag{33}$$

the power that the propeller needs in this process to expend on the mean fluid is expressed by the differential of the kinetic energy flows:

$$P_{forn} = \rho v_i A\left[\frac{1}{2}\left(U_f^2 - U_\infty^2\right)\right]U_\infty \tag{34}$$

This relations are applicable from aircraft propellers to helicopter rotors and to ascension flight in a cyclocopter.

For a hovering cyclocopter, the driving force has only to balance the weight of the cyclocopter, the approach flow velocity is now zero, and it is obtained directly from the previous relations, doing $U_\infty = 0$:

$$W = T = \rho v_i A U_f = 2\rho v_i^2 A \tag{35}$$

once that $U_j = 2U_d$

It can finally be shown the flow velocity U_d:

$$v_i = \sqrt{\frac{T}{2\rho A}} \tag{36}$$

A model described in [1] proposes a similar model with a corrective factor $k = 1.15$:

$$v_i = \sqrt{\frac{kT}{2\rho A}} \tag{37}$$

4.1.1 Double-Multiple Streamtube Model

In the double-multiple streamtube model, the rotor is divided into several tubes that cross the rotor twice with different velocity induced values in the upstream and downstream halves, as shown in Fig.7(b).

In the two intersection points of each streamtube with the blade path, the swept area ($Rd\psi$) acts as an infinitesimal surface, through which the rotor provides axial momentum to the flow. In the present formulation, in each balde location it is udes a 2D flow model.

In the upstream half, the flow enters the rotor in the radial direction and freight due to the pressure forces ($\bar{S}$) in the adjacent flow tube, so that the current tube becomes vertical. The bending of the current tube is also important to maintain the symmetry flow within the rotor. It is also assumed that the free pressure flow is reached at some point within the rotor and the velocity at that point is taken as the wake velocity (w) to the surface of the upstream actuator. The wake's velocity forms the free flow velocity on the surface of the downstream

actuator. Based on the mass conservation, momentum and energy in the streamtube, the wake's velocity o can be expressed in terms of induced velocity upstream as [1]:

$$w = \frac{2v_u}{\sin\Psi} \tag{38}$$

where

$$v_u = \sqrt{\frac{dT_u \sin^2\Psi}{2\rho R d\Psi}} \tag{39}$$

For the lower half of the rotor:

$$dT_d = 2\rho R v_d \sqrt{w^2 + 2wv_d \sin\Psi + v_d^2 d\Psi} \tag{40}$$

The equation above can be solved iteratively in order to obtain the inner velocity v_d in the lower half of the rotor. dT, u, d is obtained through the elements and blades analysis and is given by:

$$dT_u, d = \bar{F_w^A}\left(\frac{N_b d\Psi}{2\pi}\right) \tag{41}$$

where $\bar{F}_w^A$ is the force in the radial direction that will be obtained later using elements and blades analysis.

The equation 41 is obtained assuming that for a cyclocopter with N_b blades, each blade takes $(d\psi/2\pi)$ in each streamtube. A typical flow distribution using the double-multiple streamtube is shown in Fig: 10

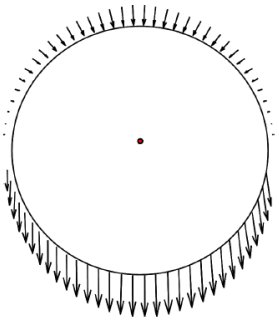

Figure 10: Example of the current flow distribution using the double-multiple streamtube model.

5. Aerodynamic Forces Calculus

The angle of attack in each section bladee is influenced by two components: (i) Wind velocity, $\overline{V}_w$, consequence of the flow entering the rotor; (ii) blade velocity, $\overline{V}_b$, in 3/4 of the chorde length, relative to the point where the blades are fixed. Not only the blade movemente but also its rotation contribute for this velocity [1].

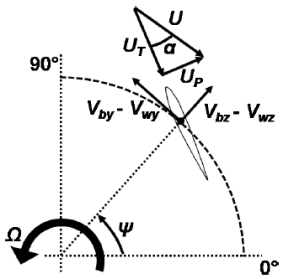

Figure 11: Scheme of the velocities used in aerodynamic formulation [1].

The general expression for the velocity resulting on the blade, clockwise, in the local referencial, will then be given by:

$$\overrightarrow{V} = -\overrightarrow{V}_w + \overrightarrow{V}_b \tag{42}$$

$\overline{V}_w$ é dado por:

$$\overrightarrow{V}_w = \overrightarrow{V}_{wx}\hat{i} + \overrightarrow{V}_{wy}\hat{j} + \overrightarrow{V}_{wz}\hat{k} \tag{43}$$

For the single streamtube model the components are:

$$V_{wy} = -v_i cos(\Psi - \beta) \tag{44a}$$

$$V_{wz} = -v_i sin(\Psi - \beta) \tag{44b}$$

For the upper part of the double-multiple streamtube model the components are given by:

$$\begin{aligned} V_{wy} &= 0, \\ V_{wz} &= -v_u, \end{aligned} \tag{45}$$

And the bottom components come given by:

$$\begin{aligned} V_{wy} &= -wcos(\Psi), \\ V_{wz} &= wsin(\Psi) + v_d \quad , \end{aligned} \tag{46}$$

Blade velocity are defined by:

$$\begin{aligned} V_{by} &= \Omega(\eta_r \sin\theta_1 + R), \\ V_{bz} &= -\Omega(\eta_r \cos\theta_1). \end{aligned} \tag{47}$$

The velocity resulting from the blades can then be written in the undeformable coordinate system, such as:

$$\begin{aligned} \overrightarrow{V} = \overrightarrow{V}_x i + \overrightarrow{V}_y j + \overrightarrow{V}_z k = \\ (V_{bx} - V_{wx})i + (V_{by} - V_{wy})j + (V_{bz} - V_{wz})k \end{aligned} \tag{48}$$

However, the loads applied to the blade section are calculated using the resulting velocity and the aerodynamic angle if attack in the rotating deformed blade coordinate system:

$$\begin{bmatrix} U_T \\ U_P \end{bmatrix} = T_{DU} \begin{bmatrix} V_y \\ V_z \end{bmatrix}, \tag{49}$$

where, U_T e U_P, are the velocities in the deformed referencial (figura 11) e T_{DU} is the transformation matrix of the undeformed referential for the deformed referencial:

$$T_{DU} = \begin{bmatrix} cos\theta_1 & sen\theta_1 \\ -sen\theta_1 & cos\theta_1 \end{bmatrix}, \tag{50}$$

$$\alpha = tan^{-1}\left(\frac{U_P}{U_T}\right), \tag{51}$$

$$U = \sqrt{U_T^2 + U_P^2}. \tag{52}$$

As seen in 3.2 the Wagner function based on the indicial aerodynamic is used to include unsteadye effects. The circulatory part of the coefficient of sustentation, C_l^c, in response to an arbitrary variation in angle of attack can then be written with a focus on Wagner's function, $\phi(s)$, as:

$$C_l^c(t) = C_{l_\alpha}\left[\alpha(0)\phi_w(s) + \int_0^s \frac{d\alpha(\sigma)}{ds}\phi(s-\sigma)d\sigma\right] \tag{53}$$

$$s = \frac{2}{c}\int_0^t U dt \tag{54}$$

Below is the approximate expression of Wagner's function for incompressible flow:

$$\phi_w(s) = 1 - A_1 e^{-b_1 s} - A_2 e^{-b_2 s} \tag{55}$$

Where $A_1 = 0.165$, $A_2 = 0.335$, $b_1 = 0.0455$ and $b_2 = 0.3$. The lifts circulatory component has the contribution of both angles of attack (α) and pitch rate, q. For an incompressible flow, the Wagner function can be used both for α as for an angular velocity. The Duhamel integral is solved by a recursive algorithm, effective variation of the angle of attack and the geometric angle, which contains wake's history, are given by:

$$\alpha_e = \alpha - X_\alpha(s) - Y_\alpha(s) \tag{56}$$

$$q_e = q - X_q(s) - Y_q(s) \tag{57}$$

where $X_\alpha(s)$ and $Y_\alpha(s)$ are recursive functions for the angle of attack, α e $X_q(s)$ and $Y_q(s)$ are recursive functions of the pitch rate, q, which are determined numerically using a recursive step in the following equations:

$$X_\alpha(s) = X_\alpha(s-\delta s)e^{-b_1\Delta s} + A_1\Delta\alpha_s \tag{58a}$$

$$Y_\alpha(s) = Y_\alpha(s-\delta s)e^{-b_2\Delta s} + A_2\Delta\alpha_s \tag{58b}$$

$$X_q(s) = X_q(s-\delta s)e^{-b_1\Delta s} + A_1\Delta q_s \tag{58c}$$

$$Y_q(s) = Y_q(s-\delta s)e^{-b_2\Delta s} + A_2\Delta q_s \tag{58d}$$

The section's lift coefficient includes both the contribution of the circulatory and non-circulatory components:

$$C_l = C_l^c + C_l^{mc} \tag{59}$$

Therefore, the lifts circulatory and non-circulatory components are given by:

$$C_l^c = C_{l\alpha}\alpha_e + \frac{1}{2}C_{l\alpha}q_e \tag{60}$$

$$C_l^{mc} = \frac{\pi}{2U}c\dot{\alpha} - \frac{\pi}{4}\left(\frac{c}{U}\right)^2 a\ddot{\alpha} \tag{61}$$

Since the rotation axis is inserted 1/4 of the chorde, $a = -0.5$. $C_{l\alpha}$ is obtained through the CFD analysis and it's equal to 5.2. However, in this analysis, corrections were applied, as observed through equation 62 to obtain the $C_{l\alpha}$ for the blades in study [1].

$$C_{l\alpha_{finite}} = \frac{C_{l_{\alpha 2D}}}{1 + \frac{C_{l_{\alpha 2D}}}{2AR\pi}} \tag{62}$$

The profile coefficient friction is given by:

$$C_{d0} = d_0 + d_1\alpha + d_2\alpha^2 \tag{63}$$

Based on the study in CFD, the static value C_{d_0} for a NACA 0012 airfoil with Reynolds number equal to 25.000, can be expressed approximately using $d_0 = 0.0334$, $d = 0$ (symmetrical profile) and $d_2 = 2.511$. The total coefficient, C_d, is given by the sum of the components C_{d_0} and C_{d_i}:

$$C_d = C_{d_0} + C_{d_i} \tag{64}$$

where C_{d_i} is given by:

$$C_{d_i} = \frac{C_l^2}{\pi 2ARe} \tag{65}$$

The Oswald efficiency, e, is assumed as 0.85. Normal forces (F_n^A) and forces in chordes diretion,(F_c^A), are given by:

$$F_n^A = 0.5\rho U^2 c(C_l\cos\alpha + C_d\sin\alpha) \tag{66}$$

$$F_c^A = 0.5\rho U^2 c(C_l\sin\alpha - C_d\cos\alpha) \tag{67}$$

In this formulation, the flow in the blade's transverse direction is ignored, and therefore, the force in the direction x, is zero, wich means, $F_x^A = 0$. The aerodynamic forces in the undeformed rotating blades coordinate system are shown as:

$$\overrightarrow{F}^A = F_u^A\hat{i} + F_v^A\hat{j} + F_w^A\hat{k} \tag{68}$$

Where:

$$\begin{bmatrix} F_u^A \\ F_v^A \\ F_w^A \end{bmatrix} = T_{DU}^T \begin{bmatrix} F_x^A \\ F_c^A \\ F_n^A \end{bmatrix} \tag{69}$$

In the non-rotational inertial system, the aerodynamic forces, F_Z^A F_Y^A, are given by:

$$F_Z^A = F_w^A \sin\Psi + F_v^A \cos\Psi \tag{70a}$$

$$F_Y^A = -F_w^A \cos\Psi + F_v^A \sin\Psi \tag{70b}$$

6. Results and Validation

In order to validate the numerical model, we used the experimental works developed in [1] and [6].

In the following graphics are represented the values obtained by the single streamtube numerical model (green lines), the experimental values obtained in [1] and [6] (blue dots) and the values obtained by the numerical model in [1] (orange). Along with the graphics, it is shown cyclorotors dimensional characteristics (blade span (b), string c, radius of rotor (R), number of blades (N_b) and the maximum geometric angle (θ_{max})).

Table 1: Cyclorotor's dimensional characteristics - Figure 12.

b (m)	c (m)	R (m)	N_b	θ_{max}
0.1524	0.0254	0.077	3	35º

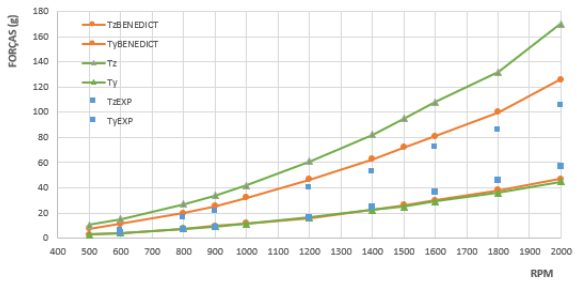

Figure 12: Forces T_z and T_y (in grams) for the experimental and numerical results as a function of the speed rotation (rpm) [1],[6].

The graphic below shows how the forces T_z and T_z evolve by increasing the blade's maximum geometric angle (max).

Table 2: Cyclorotor's dimensional characteristics - Image 13.

b (m)	c (m)	R (m)	N_b	rpm
0.1524	0.0254	0.075	3	1500

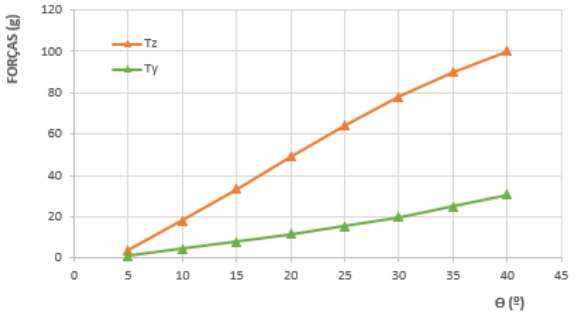

Figure 13: Forces T_z and T_y (in grams) for the numerical results as a function of the geometric angle of attack.

Table 3: Cyclorotor's dimensional characteristics - Image 14.

b (m)	c (m)	θ_{max}	N_b	rpm
0.1524	0.0254	25º	3	1500

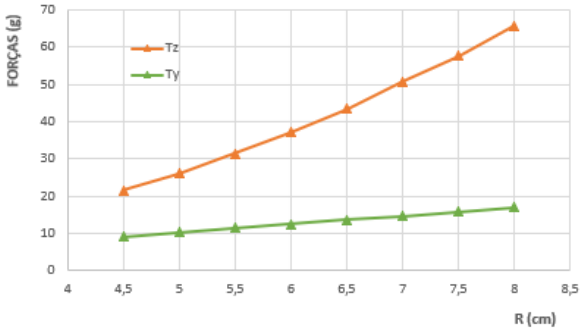

Figure 14: Forces T_z and T_y (in grams) for the numerical results as a function of the roto's radius speed (cm).

Table 4: Cyclorotor's dimensional characteristics - Figure 15.

b (m)	c (m)	R (m)	N_b	θ_{max}
0.1524	0.0254	0.07	3	30;40

7. Conclusions

From the above results, precisely from the graph of figure 12, with respect to the numerical model used, we observe that: (i) There is a considerable difference (about 30%) T_Z between the model used in this document and the single tube numerical model used in [1]; (ii) Despite this difference, the growth tendency with the increase of the rotation speed is similar to the numerical model, used in cite benedict: fund and to the experimental results; (iii) It is verified that the difference between the forces T_y for the two models is negligible; (iv) Given that

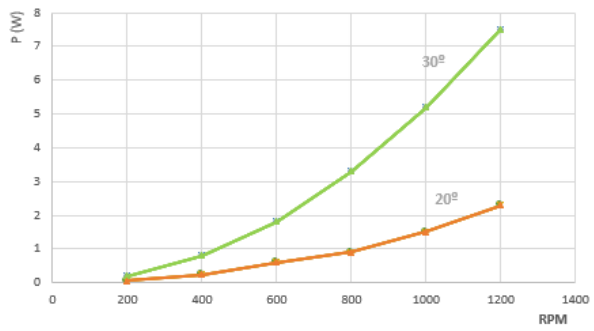

Figure 15: Power P (in Watt) for the numerical results as a function of the speed rotation (rpm).

the difference between the numerical model used in this document and the model used in cite benedict: fund differs only in the introduction of the elasticity, which is neglected in the first and it is considered in the second, it should be noted that the elasticity of the blades must be considered if the calculations are rigorous.

Relativly to the behavior of the cyclorotor and analyzing the figures 12, 13 and 14 graphics, we can conclude that: (i) Both forces (T_z and T_y) increase with increasing speed of rotation (figure 12). This sum is not proportional, and it is observed that the slope of the curve increases as the speed of rotation increases; (ii) Both forces (T_z and T_y) increase with the increase of the geometric angle of attack, max. However, this increase is not proportional, especially for the force T_z whose curve slope decreases slightly as the speed of rotation increases; (iii) Both forces, T_z and T_y, increase with increasing rotor radius, R. This increase is also not proportional, especially for the force T_z whose curve slope increases slightly as the radius increases..

References

[1] M. Benedict. FUNDAMENTAL UNDERSTANDING OF THE CYCLOIDAL-ROTOR CONCEPT FOR MICRO AIR VEHICLE APPLICATIONS. PhD thesis, Department of Aerospace Engineering, University of Maryland, 2010.

[2] M. Benedict, I. Chopra, M. Ramasamy, and J. Leishman. Performance of a cycloidal rotor concept for micro air vehicle applications. JOURNAL OF THE AMERICAN HELICOPTER SOCIETY, 55, 2010. DOI:10.4050/JAHS.55.022002.

[3] J. Sirohi, E. Parsons, and I. Chopra. Hover performance of a cycloidal rotor for a micro air vehicle. Department of Aerospace Enginnering, University of Maryland, College Park, MD.

[4] J. J. Dicker. Theory of Machines and Mechanisms. Oxford University Press, 3rd edition, 2003. ISBN:0-1-9-5-I5598-X.

[5] V. Brederode. Fundamentos de Aerodinâmica Incompressível. Edição do Autor, 1st edition, 1997. ISBN:972-97402-0-8.

[6] M. Benedict, I. Chopra, M. Ramasamy, and J. Leishman. Experimental investigation of the cycloidalrotor concept for a hovering micro air vehicle. College Park, MD 20742, April 29 – May 1 2008. Department of Aerospace Engineering University of Maryland, American Helicopter Society International.

[7] J. Leishman. Principles of Helicopter Aerodynamics. CAMBRIDGE UNIVERITY PRESS, 1st edition, 2000. ISBN:0-521-52396-6.